OPEN

NPG Asia Materials (2017) 9, e442; doi:10.1038/am.2017.187
www.nature.com/am

ORIGINAL ARTICLE

A novel ultra-thin-walled ZnO microtube cavity supporting multiple optical modes for bluish-violet photoluminescence, low-threshold ultraviolet lasing and microfluidic photodegradation

Qiang Wang[1], Yinzhou Yan[1], Feifei Qin[2], Chunxiang Xu[2], Xuelu Liu[3], Pingheng Tan[3], Nana Shi[1], Shuopeng Hu[4], Lin Li[5], Yong Zeng[1], Yan Zhao[1] and Yijian Jiang[1]

ZnO optical microcavities have shown great promise as a potential core component material/structure for ultraviolet lasers, light-emitting diodes and photonic sensors because of their outstanding optoelectronic properties. Here, we report a novel ultra-thin-walled ZnO (UTW-ZnO) microtube cavity with a wall thickness of ~750 nm, supporting multiple types of optical modes, including in-tube Fabry–Perot modes, in-wall Fabry–Perot modes and wave-guided whispering gallery modes (WG-WGMs). The free-exciton recombination rate and exciton–exciton collisions are promoted in the cavity. The intensities of near-band edge (ultravoilet (UV) light) and *X*-band (blue light) emission are therefore increased at least one order of magnitude in the temperature range of 0–500 °C. Meanwhile, the temperature-sensitive multicolor luminescence of the UTW-ZnO microtubes in the visible band from near-white to bluish-violet is demonstrated for the first time. Low-threshold UV lasing is also achieved in the UTW-ZnO microtube by WG-WGMs, where the excitation threshold is down to 5.50 μW. Furthermore, light harvesting in the microtube cavity is beneficial to boosting the ZnO catalytic performance for photodegradation of organic dyes. The UTW-ZnO microtube exhibits compatibility to microfluidic channels for recyclable on-chip degradation. The present work provides new opportunities to design novel tubular wide-bandgap semiconductor devices for a variety of optoelectronic applications in micro/nanophotonics.

NPG Asia Materials (2017) **9,** e442; doi:10.1038/am.2017.187; published online 27 October 2017

INTRODUCTION

Recent developments of optical microcavities have attracted considerable attention and added new opportunities for designing novel micro/nanophotonic devices, including single-molecule/nanoparticle sensors, on-chip ultra-low-threshold lasers and light-emitting components.[1–3] The functional material-based microcavities further provide great potential by combining inherent optical resonance and specific material properties in one platform. ZnO is one of the most intensively studied multifunctional wide-bandgap semiconductors in the past decades for UV light sources, high-speed UV photodetectors, transparent conducting electrodes, field-effect transistors, photocatalysts, chemical sensors, energy harvesting devices and so on.[4–8] It has been acknowledged as a versatile building block for micro/nano-optoelectronic applications. Recently, strong current-driven light emissions from an individual ZnO:Ga microwire with tunable visible colors, analogous to incandescent sources, have been realized, which offer a new possibility for future ZnO-based on-chip light sources via electroluminescence.[9]

ZnO naturally possesses multiple morphological structures in micron/submicron scales, covering wires, belts, combs, rods, tubes, donuts and so on, which can be synthesized by various methods.[10–12] Some of these structures have been employed as optical resonators for random, Fabry–Perot (FP) or whispering-gallery mode (WGM) UV lasing.[13–16] Particularly, FP modes and WGMs coexisting with different polarizations have been observed in an elongated hexagonal microcavity.[17] The WGMs are generally supported by the hexagonal geometry of ZnO corresponding to the crystallographic plane of (0001), providing strong optical confinement and feedback by total internal reflection (TIR) as a high-*Q* cavity.[12,15,18–21] The exciton–exciton (*ex–ex*) collision has been proposed as a substitute for electron–hole plasma as a means of lowering the threshold of lasing in ZnO microcavities.[12,21–24] The lasing threshold can be further reduced by introducing metals and graphene surface plasmons because of the high confinement of the optical fields and strong photon–exciton interactions.[25,26] The tailored geometry of the microcavity is

[1]Institute of Laser Engineering, Beijing University of Technology, Beijing, China; [2]State Key Laboratory of Bioelectronics, School of Biological Science and Medical Engineering, Southeast University, Nanjing, China; [3]State Key Laboratory of Superlattices and Microstructures, Institute of Semiconductors, Chinese Academy of Sciences, Beijing, China; [4]College of Applied Sciences, Beijing University of Technology, Beijing, China and [5]Laser Processing Research Centre, School of Mechanical, Aerospace and Civil Engineering, The University of Manchester, Manchester, UK
Correspondence: Dr Y Yan, Institute of Laser Engineering, Beijing University of Technology, No. 100 Pingleyuan, Chaoyang District, Beijing 100124, China.
E-mail: yyan@bjut.edu.cn
Received 8 June 2017; revised 19 August 2017; accepted 28 August 2017

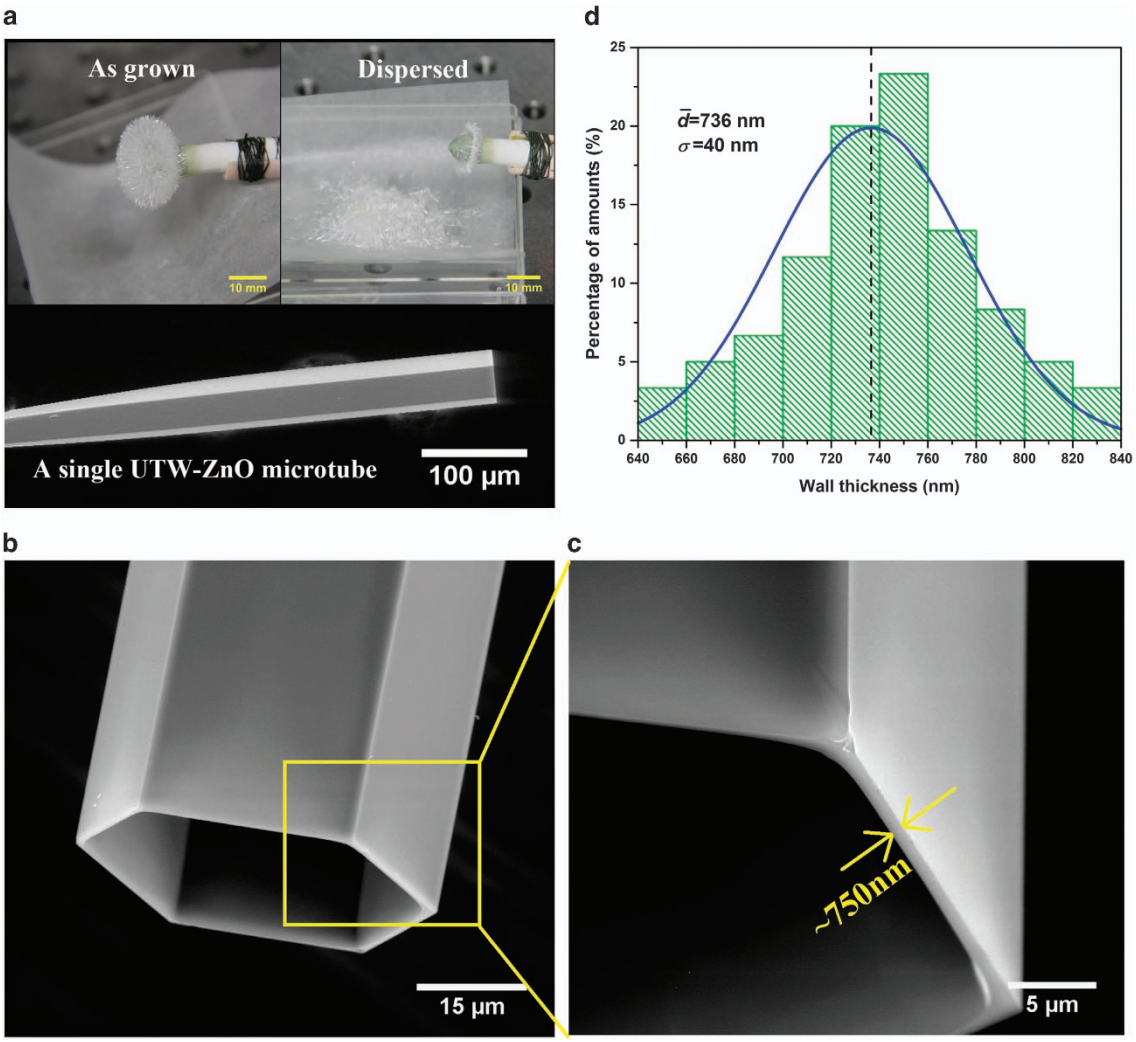

Figure 1 Morphologies of ultra-thin-walled ZnO (UTW-ZnO) single-crystal microtube. (**a**) UTW-ZnO microtubes grown on the ceramic precursor rod and scanning electron microscopic (SEM) overview of an UTW-ZnO microtube. (**b**) Close-up view of the UTW-ZnO microtube at the top end. (**c**) SEM image of the microtube facet wall. (**d**) Distribution of the wall thickness measured from 200 microtubes.

an alternative way to improve the microcavity performance by reducing the mode volume. However, few studies focus on the tailored ZnO microcavities owing to a lack of fabrication techniques. Therefore, their extraordinary optical properties in micro/nanophotonics have not been revealed comprehensively.

As a representative of tailored microcavities, a ZnO microtube cavity can be fabricated by a variety of techniques, such as microwave heating growth, aqueous solution growth and vapor-phase transport growth.[27–29] High-quality undoped acceptor-rich ZnO single-crystal microtubes were successfully fabricated in our previous work using optical vapor supersaturated precipitation (OVSP).[30] The process parameters were then optimized to grow thin-walled microtubes that were a 100 μm in diameter and a few microns thick in the facet wall with a high finish quality.[31] Although the thin-walled ZnO microtube possesses a hexagonal cross-section, the optical properties as a microcavity have not yet been studied.

Here, we demonstrate high-quality ultra-thin-walled ZnO (UTW-ZnO) single-crystal microtubes with a diameter of >50 μm and a facet wall thickness of <1 μm (i.e., the ratio of the microtube wall thickness to the diameter is <1:50). These microtubes support multiple types of optical modes, including in-tube FP modes, in-wall FP modes and wave-guided WGMs (WG-WGMs) with a high-*Q* and a small mode volume. The extraordinary optical properties of the microtube cavity are revealed and several unprecedented applications are demonstrated. This work paves new ways to develop novel on-chip tubular semiconductor devices for a variety of applications in micro/nanophotonics.

EXPERIMENTAL PROCEDURES

Fabrication of UTW-ZnO microtubes

The UTW-ZnO microtubes were fabricated by optical vapor supersaturated precipitation (OVSP), as proposed in our previous work.[30,31] A ZnO ceramic precursor rod that is 6 mm in diameter and 50 mm in length was first pre-sintered in a vertical Molysili furnace at 700 °C for 10 h. Then, the top of the precursor rod was polished to a cone with a height of 3–5 mm. The precursor rod was fixed in a four-mirror optical image furnace (10000H-HR-I-VPO-PC manufactured by Crystal Systems, Hokuto, Yamanashi, Japan) equipped with four 1500 W halogen lamps as heating sources. The carrier gas was air with a flow rate of 2 L min^{-1}. The microtube diameter and wall thickness can be precisely controlled by varying the growth parameters according to the pilot experiments.[30,31] To obtain the ZnO microtubes with

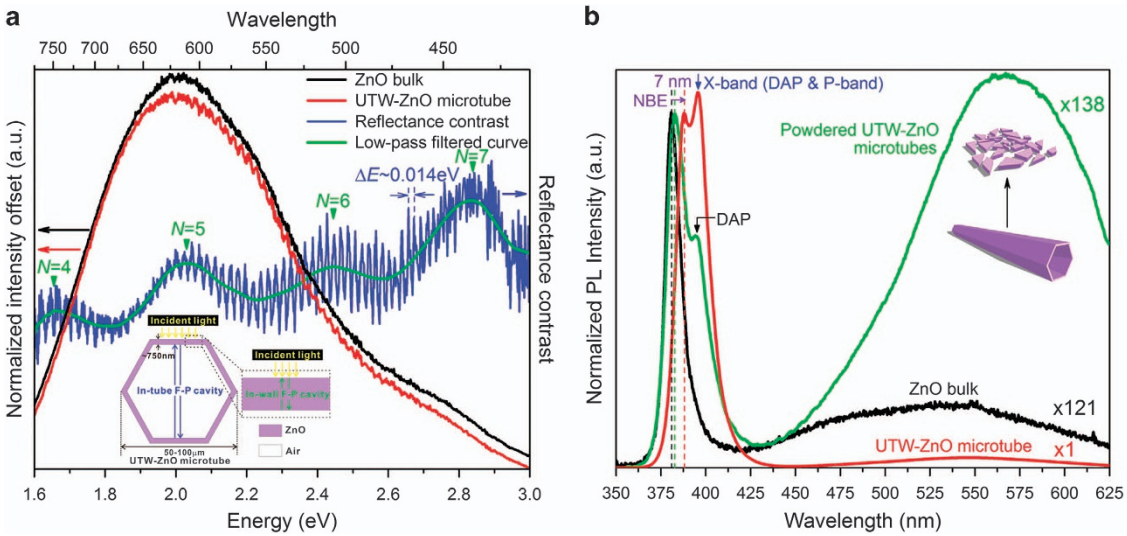

Figure 2 Optical and photoluminescence characteristics of ultra-thin-walled ZnO (UTW-ZnO) microtube optical cavity. (**a**) Reflectance and contrast spectra of the UTW-ZnO microtube with respect to the standard ZnO single-crystal bulk. (**b**) Normalized photoluminescence (PL) spectra of the UTW-ZnO microtube, ZnO single-crystal bulk and mechanically powdered ZnO microtubes (MP-ZnO microtubes).

a wall thinner than 1 μm, the lamp power was set to be 65% (of 1500 W), and the temperature holding time in the growth was increased to 2.5 h for sufficient redecomposition. The as-grown and mechanically detached microtubes from the ceramic precursor rod are shown in the insets of Figure 1a. The typical morphologies of a single microtube are shown in Figures 1a–c. The hexagonal cross-section was formed by self-assembly on the crystallographic plane of (0001) during OVSP growth of the wurtzite-type ZnO single-crystal microtubes.[30] The microtube dimensions were >5 mm in length and ~50 μm in diameter. Considering the uniform temperature field during OVSP growth, the fluctuation of the microtube wall thicknesses should be negligible. Figure 1d illustrates the distribution of wall thickness (d) measured from 200 microtubes grown with the optimum condition, where $d = 736 \pm 40$ nm.

Photoluminescence and reflectance spectra

Photoluminescence (PL) was excited by a fiber-coupled CW 325-nm He-Cd laser (Model: IK3301R-G, Kimmon Koha, Tokyo, Japan). The laser beam was focused to 100 μm in diameter by a ×14 objective lens with an NA = 0.5. The maximum excitation power on the sample surface was 7 mW and adjustable by an attenuator. The PL signals were collected by the same objective lens in a backscattering configuration and resolved by a 1200 g mm^{-1} grating. A spectrometer with a 750 mm focal length (Model: Acton SP2750, Princeton Instruments, Trenton, NJ, USA) was used to acquire the PL spectra with a resolution of 0.023 nm. For temperature-dependent PL measurements, the specimen was placed in a temperature-controlled vacuum chamber, in which the temperature was set in the range of 0–500 °C. Then, the temperature-dependent chromaticity values in the CIE color space were calculated by the acquired PL spectra.[30]

The reflectance spectra were captured via a spectrometer (Model: LabRAM-HR800, Horiba, Edison, NJ, USA) under illumination by a halogen lamp. The reflectance contrast, C_R, can be calculated by

$$C_R = \frac{R_{bg} - R_{microtube}}{R_{bg}} \quad (1)$$

where $R_{microtube}$ and R_{bg} are the reflectance spectra of the microtube and of the background substrate (i.e., ZnO single-crystal bulk), respectively, within the measured band.

Laser spectra

Lasing from an individual UTW-ZnO microtube was excited by a confocal microphotoluminescence setup (Model: BX53, Olympus, Tokyo, Japan) coupled with a 325-nm femtosecond pulsed laser (Model: Libra-F-HE, Coherent, Santa Clara, CA, USA) with the repetition rate of 1 kHz and pulse duration of 150 fs. The excitation laser was focused onto the microtube facet surface through a ×10 objective lens with a spot size of 16 μm. The spectra of the lasing emission were collected and resolved by a spectrometer (Model: Acton SP2500i, manufactured by Princeton Instruments, Trenton, NJ, USA).

Photocatalytic activity

Photodegradation of the methylene blue (MB) solution was performed using a 15 W xenon arc lamp (Model: CEL-HX F300, CeAuLight, Beijing, China) to simulate solar illumination. A total of 50 mg of the ZnO microtubes was suspended in 50 ml of the MB solution (10 mg l^{-1}) in a quartz beaker. The suspension was stirred in the dark for 2 h to achieve adsorption equilibrium on the surfaces of the microtubes. A total of 3 ml of the solution was extracted every 20 min during photodegradation for an absorbance measurement. Compared with nano-photocatalysts, there is no requirement for centrifugation due to the large size of the microtubes. The absorbance of the solution within the visible band was analyzed with a spectrophotometer (Model: UV-3600, Shimadzu, Kyoto, Japan), where the deionized water was used as the reference. The degradation percentage, η, can be calculated by

$$\eta = \frac{C_0 - C(t)}{C_0} \times 100\% = \frac{I_0 - I(t)}{I_0} \times 100\% \quad (2)$$

where I_0 is the absorbance intensity of the MB solution with an initial concentration of C_0 (10 mg l^{-1}), and $I(t)$ is the absorbance intensity of the MB solution with a concentration of $C(t)$ after photodegradation for a time t. The kinetic behavior of MB photodecomposition on the ZnO catalyst surface was estimated by the first-order kinetics model as follows:

$$\ln\left(\frac{C_0}{C}\right) = \ln\left(\frac{I_0}{I}\right) = kt \quad (3)$$

where k is the degradation rate.

Numerical simulation of WG-WGMs

The numerical simulation and eigenmode analysis of WG-WGMs in the microtube optical cavity were performed using the COMSOL Multiphysics (licensed by COMSOL, developed by COSMOL group, Stockholm, Sweden) software tool with a finite element method algorithm. A two-dimensional cross-section model was developed for electromagnetic field calculation and eigenmode analysis. The refractive indexes of ZnO, air (as the background of lasing) and water (as the background of photodegradation) near the UV band

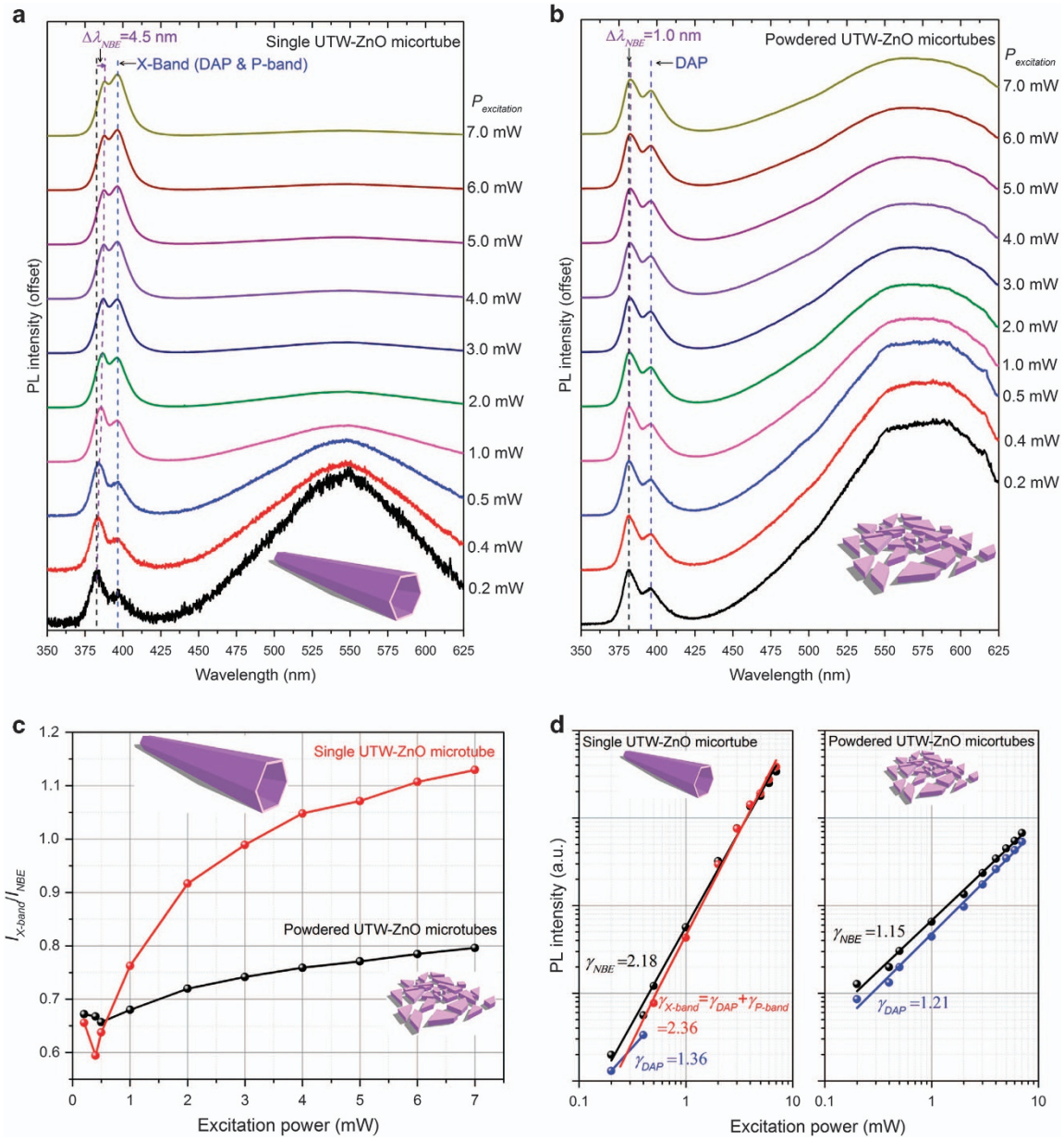

Figure 3 Excitation-power-dependent photoluminescence (PL) analysis of (**a**) an ultra-thin-walled ZnO (UTW-ZnO) microtube and (**b**) MP-ZnO microtubes. (**c**) PL intensity ratio of the *X*-band to the donor–acceptor pair (DAP) emission for the UTW-ZnO microtube and MP-ZnO microtubes. (**d**) Integrated PL intensity of the *X*-band and the DAP emissions as a function of the excitation power in double logarithmic plots.

were 2.30, 1.00 and 1.34, respectively. The perfect matching layers were applied as the open boundary conditions.

RESULTS AND DISCUSSION

Optical and PL characteristics

The reflectance spectra and contrast of the UTW-ZnO microtube with respect to the ZnO bulk are shown in Figure 2a. Figure 2a illustrates two types of FP modes supported in the UTW microtube cavity, that is, the high-frequency fringe ($\Delta E \sim 0.014$ eV) corresponding to 'in-tube' FP modes and the low-frequency fringe ($\Delta E \sim 0.415$ eV by low-pass filtering) corresponding to 'in-wall' FP modes. The cavity length $L = c/(2n\Delta\nu)$ can therefore be used to estimate the microtube diameter and wall thickness, where c is the speed of light, n is the refractive index of the cavity and $\Delta\nu$ is the frequency separation between adjacent modes calculated by $(e/h)\Delta E$, where e is the charge of an electron and h is Planck's constant. The calculated microtube diameter and wall thickness were 50 ± 10 μm and 750 ± 50 nm, respectively, in good agreement with the scanning electron microscopic measurement that is shown in Figure 1. The two FP cavities enhance the incident light confinement in the microtube and boost the spontaneous emission rate by Purcell's effect.[32] An ~120-fold enhancement of UV band emission in the UTW-ZnO microtube with respect to the ZnO bulk was therefore achieved under the same UV excitation power (7 mW), as shown in Figure 2b. The high recombination rate of the near-band edge (NBE) free excitons suppressed the deep-defect level emission at the visible band down to ~20%. The PL

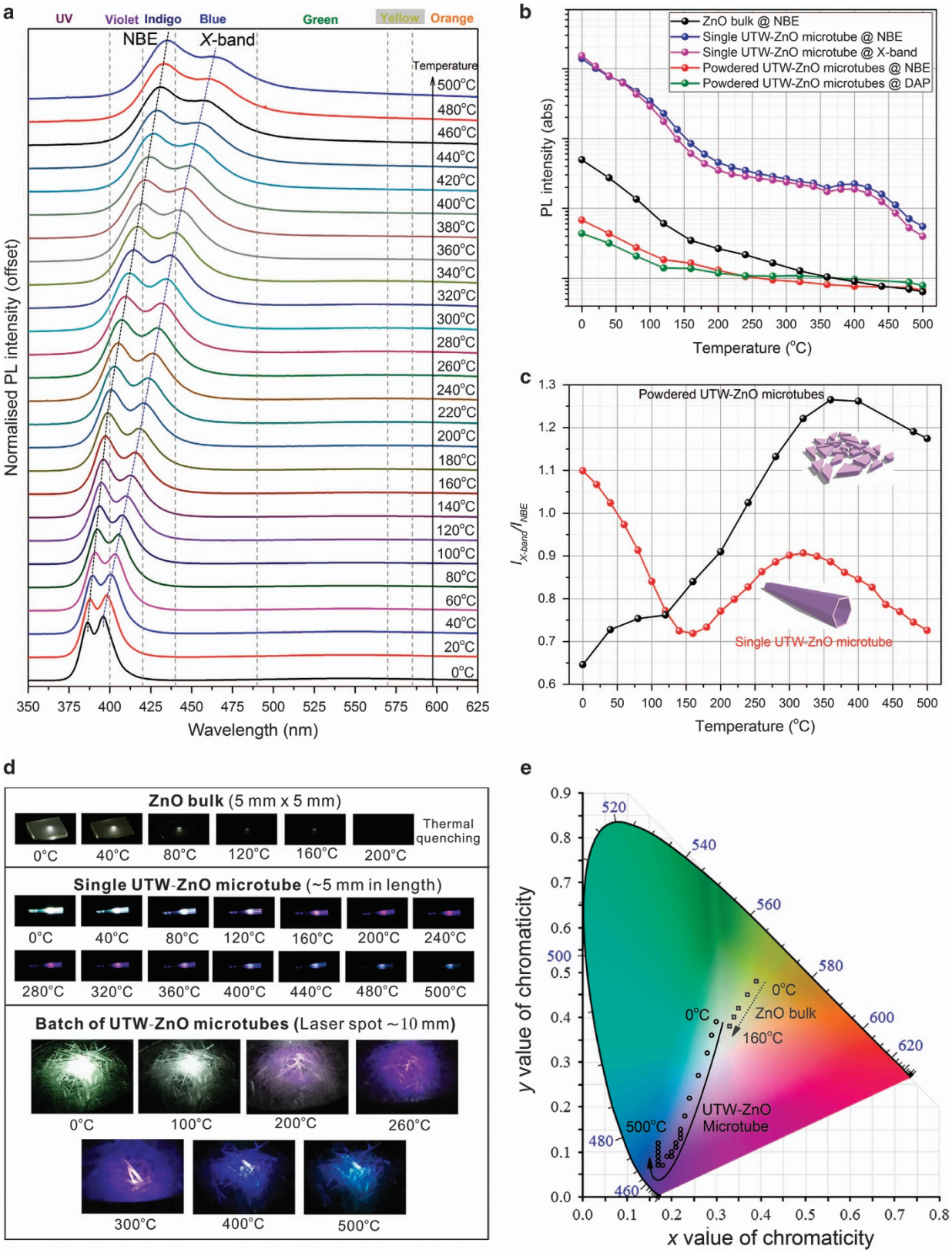

Figure 4 Temperature-dependent multicolor photoluminescence (PL). (**a**) PL spectra of a ultra-thin-walled ZnO (UTW-ZnO) microtube. (**b**) PL intensities of the near-band edge (NBE), donor–acceptor pair (DAP) and *X*-band emissions from various ZnO specimens. (**c**) Intensity ratios of the *X*-band to NBE emissions from different ZnO specimens. (**d**) Images of temperature-dependent luminescence from a ZnO single-crystal bulk, a single UTW-ZnO microtube and a batch of UTW-ZnO microtubes. (**e**) Chromaticity values of a ZnO single-crystal bulk and a single UTW-ZnO microtube luminescence in the CIE color space.

peak at ~396 nm was well acknowledged as a so-called *P*-band from *ex–ex* collisions under a high excitation intensity.[12,21–24] The redshift of the NBE emission and dual peaks near the UV band further indicated the potential of strong *ex–ex* collisions occurring in the UTW-ZnO microtube. The V_{Zn}-related donor–acceptor pair (DAP) emission at room temperature was also located in the same band for the OVSP-grown acceptor-rich ZnO microtubes.[30] To identify the contribution of *P*-band and DAP emissions, the microtubes were mechanically powdered for the purpose of destroying optical cavity structures and eliminating Purcell's effect. The reduced intensity at ~396 nm and blueshift of the NBE emission in the mechanically powdered ZnO microtubes (MP-ZnO microtubes) validated the obvious contribution of the microtube optical cavity to strengthen free-exciton recombination and *ex–ex* collisions. The remaining dual peaks near the UV band under the low-power excitation of 7 mW confirmed a large amount of Zn vacancies existing in the MP-ZnO microtubes.[30] Therefore, the PL peak at ~396 nm for the UTW-ZnO microtube grown by OVSP should be attributed to the complexes of *P*-band and DAP emissions, defined as the *X*-band, as shown in Figure 2b.

To further validate the hypothesis of the *X*-band, the excitation-power-dependent PL spectra of a single UTW-ZnO microtube and MP-ZnO microtubes were compared, as shown in Figures 3a and b. Both specimens demonstrated typical PL behaviors of the standard ZnO single crystal, that is, the intensity ratio of NBE to deep-defect emission increased with the excitation power increasing.[33] Meanwhile, the *X*-band became dominant in the UTW-ZnO microtube, where the ratio of $I_{X\text{-band}}/I_{NBE}$ was increased from 0.68 to 1.13, as shown in Figure 3c. The significant redshift of the NBE emission (~4.5 nm) further confirms the occurrence of *ex–ex* collisions. In contrast, the variation of the intensity ratio and redshift of the NBE emission were negligible for the MP-ZnO microtubes due to the optical cavity being broken. The PL intensity, I_{PL}, with respect to the excitation density, $I_{excitation}$, follows a well-known power law of $I_{PL}=I'^{\gamma}_{excitation}$. Figure 3d shows that the fitted exponents for NBE and *X*-band emissions (i.e., γ_{NBE} and $\gamma_{X\text{-band}}$) in the single UTW-ZnO microtube are 2.18 and 2.36, respectively. However, γ_{NBE} and γ_{DAP} are only 1.15 and 1.21 in the MP-ZnO microtubes. It can be deduced that the microtube optical cavity boosted the free-exciton recombination rate and the possibility of *ex–ex* collisions for *P*-band activation. The emission photon energy of the *P*-band, P_n, is identified as[12]

$$P_n = E_{ex} - E_b^{ex}\left(1-\frac{1}{n^2}\right) - \frac{3}{2}kT = E_{ex} - E_b^{ex} - \frac{3}{2}kT \,|\, n\to\infty \qquad (4)$$

where E_{ex} is the free-exciton emission energy, E_b^{ex} is the binding energy of an exciton, n is the quantum number of the excited exciton and kT is the thermal energy. The calculated energy shift of the *P*-band emission at room temperature ($n\to\infty$) was 99 meV lower than the NBE emission, in good agreement with the energy difference between the *X*-band and the NBE emission energy in the PL spectrum (~98 meV). Figure 3d also demonstrates a threshold power of 0.28 mW, above which γ was converted from being DAP dominated ($\gamma_{DAP}\sim 1.36$) to *X*-band ($\gamma_{DAP}+\gamma_{P\text{-band}} \sim 2.36$) dominated in the UTW-ZnO microtube. The excitation threshold of *P*-band activation (i.e., 0.28 mW) is significantly lower than those reported in other literatures.[12,22–24] This phenomenon is attributed to the high-quality factor and small mode volume of the UTW-ZnO microtube optical cavity, making the localized exciton states easily saturated and therefore raising the possibility of *ex–ex* collisions.[23]

Temperature-sensitive multicolor luminescence in the visible band

The outstanding property of the high NBE free-exciton recombination rate and low-threshold *X*-band activation makes the UTW-ZnO microtube cavity promising for light emission above room temperature. Figure 4a shows the temperature-dependent PL spectra of a UTW-ZnO microtube from 0 to 500 °C. The peaks of the NBE and *X*-band emissions shift from the UV to the indigo and blue region, respectively. It is well known that the exciton-related PL intensity is markedly reduced due to thermal quenching of free excitons as the temperature increases. However, the UTW-ZnO microtube cavity overcame the thermal quenching. The boosted NBE recombination rate and lowered *P*-band activation threshold due to Purcell's effect increased the intensities of the NBE and *X*-band emissions by at least one order of magnitude in the entire temperature range, as shown in Figure 4b. The temperature-dependent intensity ratio of the *X*-band to NBE emissions is shown in Figure 4c. The reduced intensity ratio in the UTW-ZnO microtube below 150 °C indicated that the *ex–ex* collisions (i.e., *P*-band) were partially quenched as the temperature increased. The variation of the intensity ratio above 150 °C was similar to that of the MP-ZnO microtubes, where the *P*-band was completely suppressed, whereas the thermal quenching of the DAP transition was lower than the NBE free-exciton recombination due to the high thermal stability of the V_{Zn}-related acceptors.[30]

The temperature-dependent PL and corresponding luminescence color in the visible band of a standard ZnO single-crystal bulk and UTW-ZnO microtubes are shown in Figures 4d and e, respectively. The typical PL color of the standard ZnO single-crystal bulk was green-yellow at room temperature due to the deep-defect level emission. The calculated chromaticity values in the CIE color space were (0.39, 0.48) and shifted to near-white (0.33, 0.38) with the temperature increase to 160 °C, above which the luminescence vanished due to thermal quenching, as shown in the top panel of Figure 4d. In UTW-ZnO microtubes, the luminescence in the visible band was remained up to 500 °C, indicating a high spontaneous emission rate in the microtube cavity. The luminescence color was near-white at room temperature that was attributed to the tail of the DAP emission located in the purple region and to the deep-defect level emission in the green-yellow region. With the elevation of the temperature, the high intensities of the NBE and DAP emissions with obvious redshifts tuned the luminescence color within the visible band from near-white (0.30, 0.39) to purple (0.17, 0.07) and then to bluish violet (0.17, 0.12) up to 500 °C, as shown in the middle panel of Figures 4d and e. To demonstrate the luminescence efficiency, a batch of microtubes was excited by an unfocused UV laser with a spot diameter of 10 mm (excitation intensity ~0.01 W cm^{-2}). The bottom panel of Figure 4d indicates that the PL was still detectable by the camera up to 500 °C and the luminescent colors were consistent with a single UTW-ZnO microtube excited by the focused UV laser. The extraordinary temperature-sensitive multicolor luminescence in the visible band would make the UTW-ZnO microtubes suitable as high-efficient color-tunable inorganic fluorescence sources for high temperature usage.

WG-WGMs for low-threshold UV lasing

The room temperature UV lasing from a single UTW-ZnO microtube was carried out using a 325-nm femtosecond (fs) pulsed laser. Figure 5a exhibits the emission spectra at various excitation powers. At a pumping power lower than ~5.60 μW, the spectrum only presents a broad *X*-band emission. When the excitation power was >5.60 μW, sharp emission peaks appeared with a rapid increase of intensities indicating the conversion from spontaneous emission to

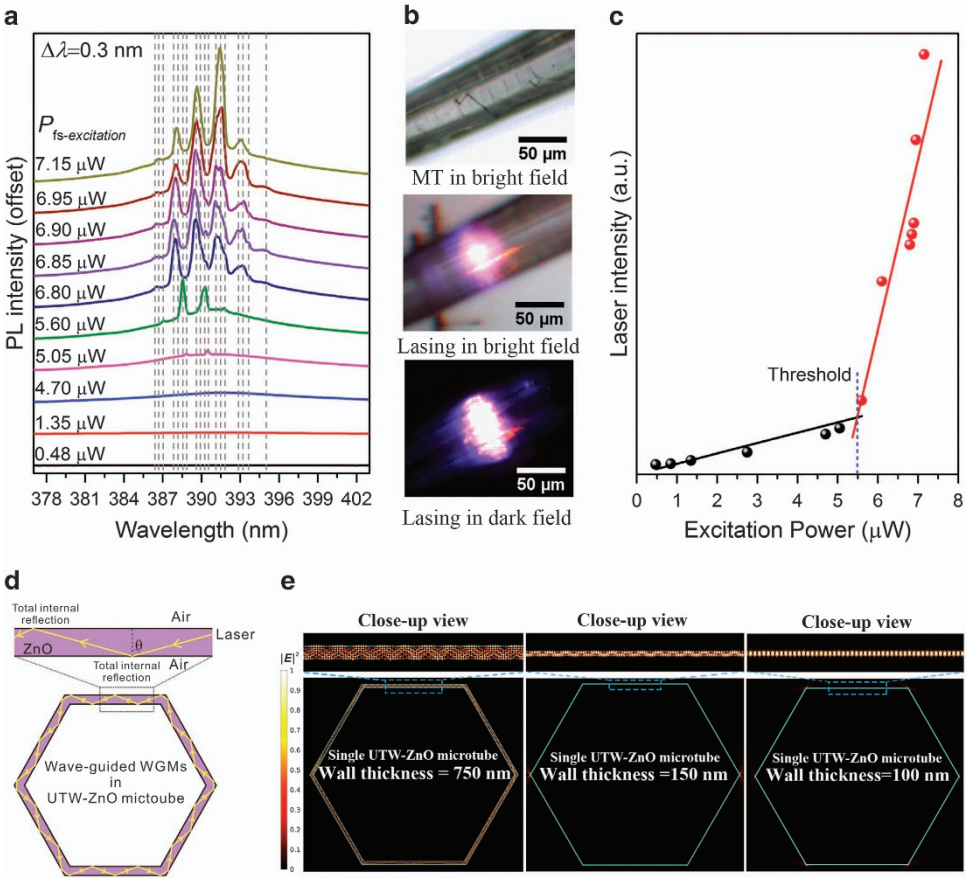

Figure 5 Ultraviolet (UV) lasing from an ultra-thin-walled ZnO (UTW-ZnO) microtube optical cavity. (**a**) Laser emission spectra under various excitation powers. (**b**) UTW-ZnO microtube and laser emission in bright and dark fields. (**c**) Evolution of lasing intensity with excitation power. (**d**) Schematic diagram of wave-guided whispering gallery modes (WG-WGMs) in a UTW-ZnO microtube via total internal reflection. (**e**) Numerical simulation of WG-WGMs in UTW-ZnO microtubes with various wall thicknesses.

stimulated one. Figure 5b shows the image of shiny violet light confined in the UTW-ZnO microtube optical cavity. According to the transition point of the laser intensity, as shown in Figure 5c, the lasing threshold was determined as 5.50 μW. The mode spacing ($\Delta\lambda = 0.3$ nm) was significantly smaller than the 'in-tube' or 'in-wall' FP modes, for which the spacing was ~1.7 and ~120 nm, respectively, in the band near 390 nm. A long cavity should be considered for UV lasing with a small mode spacing. Considering the light scattering of the in-tube and in-wall modes in their own cavities, the scattered light could propagate within the thin facet walls and form the WG-WGMs by TIR, as shown in Figure 5d. The corresponding mode spacing, $\Delta\lambda$, can therefore be determined by

$$\Delta\lambda = \frac{\lambda^2}{L\left(n - \lambda\frac{dn}{d\lambda}\right)} \approx \frac{\lambda^2}{3\times\frac{d}{\sin(\theta)}\times\left(n - \lambda\frac{dn}{d\lambda}\right)} \quad (5)$$

where L is the round-trip distance of a cavity mode that can be estimated by $L = 3d/\sin\theta$, n is the refractive index of the cavity, d is the diameter of the UTW-ZnO microtube, $dn/d\lambda$ is the dispersion relation, λ is the laser wavelength and θ is the incident angle of TIR at the ZnO–air interface supporting WG-WGMs in the microtube cavity, as shown in Figure 5d. According to the numerical simulation, θ was ~40° for the microtube with a diameter of 50 μm and a wall thickness of 750 nm. The cavity length, L, was calculated to be 233.28 μm. According to Equation (5), the mode spacing was ~0.32 nm in good agreement with the experimental result (i.e., ~0.3 nm, shown in Figure 5a) and significantly smaller than that in micron-sized ZnO cavities.[15,19] However, the Q factor of the microtube cavity ($Q \sim 10^3$) resulted in the full-width at half-maximum of the laser peak (~0.39 nm) being slightly greater than the mode spacing. Laser mode competition and depletion could therefore occur, by which several peaks were suppressed under various excitation powers, as shown in Figure 5a.

The low lasing threshold in the UTW-ZnO microtube was attributed to the high gain threshold determined by $G_{th} \propto 1/\beta l$, where β is the gain and l is the cavity length.[11,34] The ultralow excitation intensity for P-band activation confirmed the high gain in the microtube cavity.[12,22,23] The WG-WGMs at the tubular cross-section increased the equivalent cavity length by TIR, as shown in Figure 5d. Additionally, the contribution of the mode volume to the lasing threshold cannot be ignored in the UTW cavity. It is well known that the strength of photon–exciton interaction was determined by the Q factor in the time domain and by the mode volume in the spatial domain. The small mode volume promised high light confinement in the microtube wall for enhancement of free-exciton recombination by Purcell's effect.[32] The mode volume of the UTW-ZnO microtube cavity with a diameter of 50 μm and a facet wall thickness of 750 nm was smaller by two orders of magnitude than the microrod with the same diameter. As a result, the lasing threshold for the UTW-ZnO microtube was markedly lowered due to the cavity length being close to the tubular circumference and the small mode volume within the

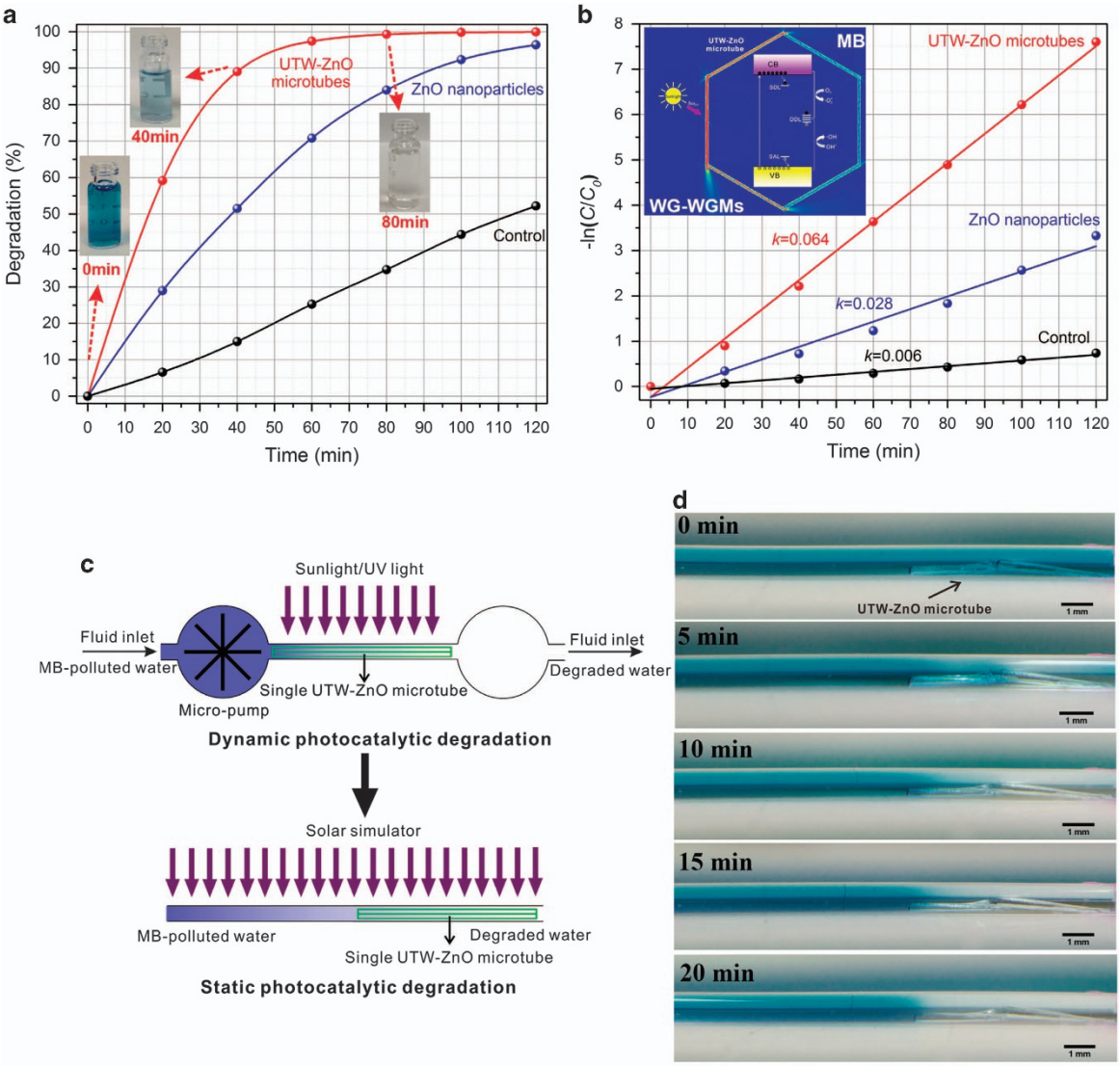

Figure 6 Photocatalytic performance of ultra-thin-walled ZnO (UTW-ZnO) microtubes. (**a**) Evolution of degradation with solar illumination time using UTW-ZnO microtubes and commercial ZnO nanoparticles. (**b**) The first-order kinetics of methylene blue (MB) photodegradation on UTW-ZnO microtubes' and nanoparticles' surfaces. Inset: schematic diagram of photocatalytic mechanisms of UTW-ZnO microtubes. (**c**) Two typical setups of on-chip photodegradation using a single UTW-ZnO microtube. (**d**) UTW-ZnO microtube photodegradation of high-concentration MB solution filling a glass capillary.

thin facet wall. Figure 5e demonstrates the typical WG-WGMs in various facet wall thicknesses. For facet wall thicknesses down to 100 nm, the incident angle of TIR was ~90° and the WG-WGMs were degenerated to the conventional ones (i.e., travelling-wave WGMs). In this case, the maximum mode spacing (i.e., $\sin\theta \sim 1$) with the minimum mode volume was realized and the lowest lasing threshold was achieved. The WG-WGMs in UTW-ZnO microtubes provided an alternative approach to designing novel UV microlasers with a low threshold.

Enhanced photocatalytic performance for recyclable on-chip degradation

In addition to light/laser sources, ZnO has been widely used as a catalyst for photodegradation of organic dyes. Previous studies generally focused on the material rather than the optical properties of ZnO for improvement of degradation efficiency.[35–37] The capabilities of photocatalytic degradation for MB by the UTW-ZnO microtubes and commercial ZnO nanoparticles were compared under solar simulator illumination (AM 1.5) with 700 mW cm^{-2}. Figure 6a shows the evolution of the degradation percentage (η) with illumination time for various ZnO catalysts. The values of η reach 99.3%, 84% and 34.7% for the UTW-ZnO microtubes, ZnO ceramic nanoparticles and control, respectively, at 80 min. The UTW-ZnO microtubes exhibited the highest photocatalytic activity, although their sizes are much greater than the nanoparticles. The degradation rates (k) for various catalysts are fitted in Figure 6b. The photodegradation rate of the UTW-ZnO microtube (0.067 min^{-1}) was 200% higher than the commercial nanoparticles (0.030 min^{-1}). Considering the dimensions of the UTW-ZnO microtube that was tens of microns in diameter and millimeters in length, the photocatalytic enhancement should be attributed to three channels, as shown in the inset of Figure 6b. (i) UV light harvesting by the microtube optical cavity (including WG-WGMs, in-tube FP modes and in-wall FP modes) causing more free-excitons participation in the photocatalytic reaction. (ii) The thin

facet wall of the microtube providing a greater ratio of surface area to volume for adsorption of MB molecules. (iii) The UTW-ZnO microtube grown by OVSP with massive stable V_{Zn}-related shallow acceptors severing as active sites that coexist with instinct donors, deep defects, the valence band and the conduction band leading to extra oxidation–reduction reactions.[30,38,39] Additionally, the large dimensions of the UTW-ZnO microtubes suppressed photocorrosion during degradation.[40] UTW-ZnO microtubes can therefore be used as a recyclable and durable photocatalyst in microfluidic channels for on-chip degradation. Figure 6c demonstrates a typical dynamic photocatalytic microchannel schematic. The MB solution can be photodegraded while flowing through the UTW-ZnO microtube. In this work, a localized static photodegradation setup was employed, where a microtube was placed at the end of the glass capillary and the MB solution with a high concentration of 100 mg l^{-1} (i.e., 10 times the standard concentration) filled the glass capillary. The process of photodegradation is shown in Figure 6d, where the degradation only occurred for the segments near microtubes and finished within ~20 min. The photocatalytic performance was non-deteriorated after tens of repeated cycling uses, demonstrating that the UTW-ZnO microtubes are compatible with microfluidic chips for recyclable on-chip degradation with a high efficiency.

CONCLUSION

The UTW-ZnO single-crystal microtube with a diameter of ~50 μm and a facet wall thickness of ~750 nm was fabricated in this work as a novel tailored microcavity that supports various optical modes, for example, in-tube FP modes, in-wall FP modes and WG-WGMs. The NBE emission intensity was boosted by approximately two orders of magnitude and the *P*-band was activated down to ~0.28 mW in the microtube cavity. The intensities of the near-band edge (UV light) and *X*-band (blue light) emissions with significant redshifts were increased by at least one order of magnitude in the temperature range of 0–500 °C. The temperature-sensitive luminescence in the visible band from near-white (0.30, 0.39) to bluish-violet (0.17, 0.12) was achieved for the first time. UV lasing was also realized in the single UTW-ZnO microtube under an unprecedented low threshold of 5.50 μW, due to the promoted *ex–ex* collisions in the high-*Q* and small mode volume microtube cavity. Furthermore, the UTW-ZnO microtubes with a high photocatalytic performance by multiple cavity modes and rich shallow acceptors were introduced for the degradation of organic dyes. Their compatibility with microfluidic channels for recyclable on-chip-degradation was demonstrated. The MB photodegradation rate by the UTW-ZnO microtubes was 200% higher than that by the commercial ZnO nanoparticles. The present work explored extraordinary optical properties and potential applications of the UTW-ZnO microtube as an optical cavity. It provides a novel platform for the design of low-threshold UV microlasers, temperature-sensitive multicolor light sources, enhanced on-chip photocatalysts and other tubular wide-bandgap semiconductor devices for a variety of optoelectronic applications in the future.

CONFLICT OF INTEREST

The authors declare no conflict of interest.

ACKNOWLEDGEMENTS

We acknowledge support by the National Natural Science Foundation of China (Grant Nos 11674018, 11504012), the Beijing Nova Program (Grant No. Z171100001117101) and the Scientific Research General Program of Beijing Municipal Commission of Education (Grant No. KM20150005013).

PUBLISHER'S NOTE

1 Jiang, X. F., Xiao, Y. F., Zou, C. L., He, L., Dong, C. H., Li, B. B. & Gong, Q. Highly unidirectional emission and ultralow-threshold lasing from on-chip ultrahigh-*Q* microcavities. *Adv. Mater.* **24**, OP260–OP264 (2012).
2 Shao, L., Jiang, X. F., Yu, X. C., Li, B. B., Clements, W. R., Vollmer, F., Wang, W., Xiao, Y. F. & Gong, Q. Detection of single nanoparticles and lentiviruses using microcavity resonance broadening. *Adv. Mater.* **25**, 5616–5620 (2013).
3 Baaske, M. D., Foreman, M. R. & Vollmer, F. Single-molecule nucleic acid interactions monitored on a label-free microcavity biosensor platform. *Nat. Nanotechnol.* **9**, 933–939 (2014).
4 Bao, J., Zimmler, M. A., Capasso, F., Wang, X. & Ren, Z. F. Broadband ZnO single-nanowire light-emitting diode. *Nano Lett.* **6**, 1719–1722 (2006).
5 Zhang, X., Huang, X., Li, C. & Jiang, H. Dye-sensitized solar cell with energy storage function through PVDF/ZnO nanocomposite counter electrode. *Adv. Mater.* **25**, 4093–4096 (2013).
6 Nasr, B., Wang, D., Kruk, R., Rösner, H., Hahn, H. & Dasgupta, S. High-speed, low-voltage, and environmentally stable operation of electrochemically gated zinc oxide nanowire field-effect transistors. *Adv. Funct. Mater.* **23**, 1750–1758 (2013).
7 Liu, X., Gu, L., Zhang, Q., Wu, J., Long, Y. & Fan, Z. All-printable band-edge modulated ZnO nanowire photodetectors with ultra-high detectivity. *Nat. Commun.* **5**, 4007 (2014).
8 Hu, K., Teng, F., Zheng, L., Yu, P., Zhang, Z., Chen, H. & Fang, X. Binary response Se/ZnO *p–n* heterojunction UV photodetector with high on/off ratio and fast speed. *Laser Photonics Rev.* **11**, 1600257 (2017).
9 Jiang, M., He, G., Chen, H., Zhang, Z., Zheng, L., Shan, C., Shen, D. & Fang, X. Wavelength-tunable electroluminescent light sources from individual Ga-doped ZnO microwires. *Small* **13**, 1604034 (2017).
10 Wang, Z. L. Zinc oxide nanostructures: growth, properties and applications. *J. Phys. Condens. Mater.* **16**, R829–R858 (2004).
11 Gargas, D. J., Moore, M. C., Ni, A., Chang, S. W., Zhang, Z., Chuang, S. L. & Yang, P. Whispering gallery mode lasing from zinc oxide hexagonal nanodisks. *ACS Nano* **4**, 3270–3276 (2010).
12 Chen, R., Ling, B., Sun, X. W. & Sun, H. D. Room temperature excitonic whispering gallery mode lasing from high-quality hexagonal ZnO microdisks. *Adv. Mater.* **23**, 2199–2204 (2011).
13 Cao, H., Zhao, Y. G., Ho, S. T., Seelig, E. W., Wang, Q. H. & Chang, R. P.H. Random laser action in semiconductor powder. *Phys. Rev. Lett.* **82**, 2278–2281 (1999).
14 Xu, X., Brossard, F. S., Williams, D. A., Collins, D. P., Holmes, M. J., Taylor, R. A. & Zhang, X. Mapping cavity modes of ZnO nanobelts. *Appl. Phys. Lett.* **94**, 231103 (2009).
15 Dai, J., Xu, C. X., Zheng, K., Lv, C. G. & Cui, Y. P. Whispering gallery-mode lasing in ZnO microrods at room temperature. *Appl. Phys. Lett.* **95**, 241110 (2009).
16 Dong, H., Zhou, B., Li, J., Zhan, J. & Zhang, L. Ultraviolet lasing behavior in ZnO optical microcavities. *J. Materiomics* DOI:10.1016/j.jmat.2017.06.001 (2017).
17 Dong, H., Liu, Y., Sun, S., Li, J., Zhan, J., Chen, Z. & Zhang, L. Geometry dependent evolution of the resonant mode in ZnO elongated hexagonal microcavity. *Sci. Rep.* **6**, 19273 (2016).
18 Czekalla, C., Sturm, C., Schmidt-Grund, R., Cao, B., Lorenz, M. & Grundmann, M. Whispering gallery mode lasing in zinc oxide microwires. *Appl. Phys. Lett.* **92**, 241102 (2008).
19 Dong, H., Sun, L., Xie, W., Zhou, W., Shen, X. & Chen, Z. Facile synthesis and ultraviolet lasing properties of ZnO microtubes. *J. Phys. Chem. C* **114**, 17369–17373 (2010).
20 Dong, H., Chen, Z., Sun, L., Xie, W., Tan, H. H., Lu, J. & Shen, X. Single-crystalline hexagonal ZnO microtube optical resonators. *J. Mater. Chem.* **20**, 5510–5515 (2010).
21 Xu, C., Dai, J., Zhu, G., Zhu, G., Lin, Y., Li, J. & Shi, Z. Whispering-gallery mode lasing in ZnO microcavities. *Laser Photonics Rev.* **8**, 469–494 (2014).
22 Tang, Z. K., Wong, G. K., Yu, P., Kawasaki, M., Ohtomo, A., Koinuma, H. & Segawa, Y. Room-temperature ultraviolet laser emission from self-assembled ZnO microcrystallite thin films. *Appl. Phys. Lett.* **72**, 3270–3272 (1998).
23 Sun, H. D., Makino, T., Tuan, N. T. & Segawa, Y. Stimulated emission induced by exciton–exciton scattering in ZnO/ZnMgO multiquantum wells up to room temperature. *Appl. Phys. Lett.* **77**, 4250–4252 (2000).
24 Huang, M. H., Mao, S., Feick, H., Yan, H., Wu, Y., Kind, H. & Yang, P. Room-temperature ultraviolet nanowire nanolasers. *Science* **292**, 1897–1899 (2001).
25 Li, J., Lin, Y., Lu, J., Xu, C., Wang, Y., Shi, Z. & Dai, J. Single mode ZnO whispering-gallery submicron cavity and graphene improved lasing performance. *ACS Nano* **9**, 6794–6800 (2015).
26 Abiyasa, A. P., Yu, S. F., Lau, S. P., Leong, E. S. & Yang, H. Y. Enhancement of ultraviolet lasing from Ag-coated highly disordered ZnO films by surface-plasmon resonance. *Appl. Phys. Lett.* **90**, 231106 (2007).
27 Cheng, J., Zhang, Y. & Guo, R. ZnO microtube ultraviolet detectors. *J. Cryst. Growth* **310**, 57–61 (2008).

28 Wei, A., Sun, X. W., Xu, C. X., Dong, Z. L., Yang, Y., Tan, S. T. & Huang, W. Growth mechanism of tubular ZnO formed in aqueous solution. *Nanotechnology* **17**, 1740–1744 (2006).
29 Sun, T. & Qiu, J. Fabrication of ZnO microtube arrays via vapor phase growth. *Mater. Lett.* **62**, 1528–1531 (2008).
30 Wang, Q., Yan, Y., Zeng, Y., Lu, Y., Chen, L. & Jiang, Y. Free-standing undoped ZnO microtubes with rich and stable shallow acceptors. *Sci. Rep.* **6**, 27341 (2016).
31 Wang, Q., Yan, Y., Zeng, Y. & Jiang, Y. Experimental and numerical study on growth of high-quality ZnO single-crystal microtubes by optical vapor supersaturated precipitation method. *J. Cryst. Growth* **468**, 638–644 (2017).
32 Vahala, K. J. Optical microcavities. *Nature* **424**, 839–846 (2003).
33 Cheng, H. M., Hsu, H. C., Tseng, Y. K., Lin, L. J. & Hsieh, W. F. Raman scattering and efficient UV photoluminescence from well-aligned ZnO nanowires epitaxially grown on GaN buffer layer. *J. Phys. Chem. B* **109**, 8749–8754 (2005).
34 Bagnall, D. M., Chen, Y. F., Zhu, Z., Yao, T., Koyama, S., Shen, M. Y. & Goto, T. Optically pumped lasing of ZnO at room temperature. *Appl. Phys. Lett.* **70**, 2230–2232 (1997).
35 Cao, X., Zeng, H., Wang, M., Xu, X., Fang, M., Ji, S. & Zhang, L. Large scale fabrication of quasi-aligned ZnO stacking nanoplates. *J. Phys. Chem. C* **112**, 5267–5270 (2008).
36 Zhang, L., Yin, L., Wang, C., Lun, N. & Qi, Y. Sol–gel growth of hexagonal faceted ZnO prism quantum dots with polar surfaces for enhanced photocatalytic activity. *ACS Appl. Mater. Inter.* **2**, 1769–1773 (2010).
37 Fu, M., Li, Y., Lu, P., Liu, J. & Dong, F. Sol–gel preparation and enhanced photocatalytic performance of Cu-doped ZnO nanoparticles. *Appl. Surf. Sci.* **258**, 1587–1591 (2011).
38 Lai, Y., Meng, M., Yu, Y., Wang, X. & Ding, T. Photoluminescence and photocatalysis of the flower-like nano-ZnO photocatalysts prepared by a facile hydrothermal method with or without ultrasonic assistance. *Appl. Catal. B* **105**, 335–345 (2011).
39 Zheng, Y., Chen, C., Zhan, Y., Lin, X., Zheng, Q., Wei, K. & Zhu, Y. Luminescence and photocatalytic activity of ZnO nanocrystals: correlation between structure and property. *Inorg. Chem.* **46**, 6675–6682 (2007).
40 Zhang, L., Cheng, H., Zong, R. & Zhu, Y. Photocorrosion suppression of ZnO nanoparticles via hybridization with graphite-like carbon and enhanced photocatalytic activity. *J. Phys. Chem. C* **113**, 2368–2374 (2009).